

Submitted to the *Astronomical Journal***First lensed quasar system(s) from the VST-ATLAS survey: one quad and three nearly identical pairs**Paul L. Schechter¹*MIT Kavli Institute for Astrophysics and Space Research, Cambridge, MA 02139*

Nicholas D. Morgan

Staples High School, Westport CT

B. Chehade

Durham University

N. Metcalfe

Durham University

T. Shanks

*Durham University*Michael McDonald¹*MIT Kavli Institute for Astrophysics and Space Research, Cambridge, MA 02139***ABSTRACT**

We have analyzed images from the VST ATLAS survey to identify candidate gravitationally lensed quasar systems in a sample of WISE sources with $W1 - W2 > 0.7$. Results from followup spectroscopy with the Baade 6.5 m telescope are presented for seven systems. One of these is a quadruply lensed quasar. Two are projected superpositions of two quasars at different redshifts. In one system two quasars, though at the same redshift, have very different emission line profiles, and constitute a physical binary. In three systems the component spectra are consistent with the lensing hypothesis, after allowing for micro-lensing. But as no lensing galaxy is detected in these three, we classify them as *nearly identical quasar pairs*. More extensive observations are needed to establish whether they are lensed quasars or physical binaries.

*This paper includes data gathered with the 6.5 meter Magellan telescopes located at Las Campanas Observatory, Chile.

¹MIT Department of Physics

Subject headings: AGN: quasars — gravitational lensing: strong, micro

1. Introduction

Doubly and quadruply lensed quasar systems are valuable for widely disparate purposes. Treu and Marshall (2016) present a current survey of the use of time delay measurements for cosmography. The micro-lensing of lensed quasars can be used to determine sizes for the emitting regions of quasars (Rauch and Blandford 1991; Agol and Krolik 1999; Pooley et al, 2007; Blackburne et al 2011) and to measure the dark matter fraction in lensing galaxies (Schechter and Wambsganss 2004, Pooley et al 2012, Jimenez Vicente et al 2015). For each these efforts the accuracy achieved is limited by the relatively small number of lensed systems.

The most productive lensed quasar discovery program to date has been the Sloan Digital Sky Survey Quasar Lens Search, henceforth SQLS (Inada et al. 2012), which yielded a “statistical” sample of 26 lensed quasar systems brighter than a limiting magnitude $i_{lim} = 19.1$ over 8000 square degrees in the redshift range $0.6 < z < 2.2$. An additional 36 systems that did not satisfy all of the selection criteria were also catalogued. Of these 40 were newly identified.

The ATLAS survey, carried out with VLT Survey Telescope (Shanks et al. 2015) promises to yield comparable if not greater numbers of lensed quasar systems. Its *ugriz* limiting magnitudes are nearly identical to those of SDSS. While its *ugriz* photometry covers only 4500 square degrees, the typical ATLAS seeing is 3/4 that of SDSS (Shanks et al. 2015), permitting the discovery of closer lensed quasar systems.

We have undertaken a search for lensed quasars in the ATLAS survey, and report here the first newly discovered system, a quadruply lensed quasar and three systems that have two nearly identical quasar spectra but for which no lensing galaxy has been detected.

In §2 we outline our method for identifying candidate lensed quasar systems, using the WISE catalog and ATLAS *ugriz* cutouts to choose candidates for spectroscopic and direct imaging followup. The method will be described in greater detail in a forthcoming paper. In §3 we describe direct imaging and spectroscopic followup observations of seven candidate systems obtained with IMACS on the Baade 6.5 m telescope of the Magellan Observatory. In §4 we analyze these observations. In §5 we present simple models for the the newly discovered quadruple system, WISE 2344-3056. In §6 we discuss our results.

2. Selection of Candidate Lensed Quasar Systems

2.1. Colors for marginally resolved lensed quasar systems

The colors derived for an object from a survey like ATLAS involve a number of implicit assumptions. Bright objects that are deemed point sources are used to determine a point spread function (PSF) appropriate to the exposure, usually dominated by the atmospheric seeing. Sources that appear extended with respect to this PSF might be fit with a Sersic (1963) profile. For sources that do not appear to be extended, one uses the adopted PSF to calculate a magnitude.

A gravitationally lensed quasar system is a composite object consisting of multiple images of a quasar and one or more lensing galaxies. Typical image separations are, to within a factor of two, $\sim 1''$. It is unfortunate that the typical seeing in a survey like ATLAS is also of order one arcsecond. Were it very much better, one would detect the components of the lensed quasar as distinct objects and compute colors for each. Were it very much worse, one might treat the system as a point source.¹

When the resolution of a survey is *comparable* to the image separation, the magnitudes derived for composite systems suffer systematic errors from the mismatch between the assumed PSF and the object. Moreover these systematic errors will vary with the seeing. While one might hope to select lensed quasars using their catalogued colors, systematic errors may cause systems to be missed.

The resolution of the WISE survey (Wright et al. 2010) is substantially worse than that of ATLAS, and WISE magnitudes for all but the widest lensed quasar systems do not suffer from marginal resolution. Our approach is therefore to make a first level selection based only on WISE colors. This produces a candidate list sufficiently small that one can then retrieve the ATLAS survey images for each remaining object and determine whether they are consistent with its being a system of two or more sources. Magnitudes are then computed by adopting the same image configuration for all filters, thereby mitigating the systematic errors associated with marginally resolved systems.

2.2. W1 - W2 color selection

Stern et al (2012) have shown that the WISE $W1 - W2$ color ($m_{3.6\mu} - m_{4.5\mu}$) can be used to isolate quasars from stars, and, to a lesser extent, from galaxies. The underlying explanation is that the optical light from a quasar is thermal emission from an extended region with a range of temperatures, in which case the red tail of the distribution is redder than a blackbody Rayleigh-

¹One might in principle convolve survey images with a broadening function, perhaps blurring those taken in different filters to a common PSF, and produce a catalog for the smeared data, but only with the expenditure of considerable resources.

Jeans spectrum. We adopted a criterion, $W1 - W2 > 0.70$, that struck a balance between including lensed quasar systems and isolating them from other objects. Eighty percent of the confirmed SQLS lensed quasar systems satisfy this criterion. Lensing galaxies have bluer $W1 - W2$ colors than quasars. Systems in which the light from the lens dominates that to the quasars will not be included in our sample. The fraction of SQLS quasar systems that are bluer than our criterion is larger for the fainter systems. To keep the number of candidates manageable, we limited our sample to objects with $W1 < 15$ or $W2 < 14.45$.

In the south galactic cap, ATLAS covers a region with $21^h30^m < \text{RA} < 4^h00^m$ and $-40^\circ < \text{Dec} < -10^\circ$ in the *ugriz* filters (Shanks et al 2015). In the north it covers a region with $10^h00 < \text{RA} < 15^h30^m$ and $-20^\circ < \text{Dec} < -2.5^\circ$. A second northern region with $10^h00^m < \text{RA} < 15^h00^m$ and $-30^\circ < \text{Dec} < -25^\circ$ is being surveyed in *i* and *z*, with *ugr* observations being carried out under Chilean auspices. ATLAS survey data in at least one filter was available, as of mid-March 2016, for 144,700 unique sources that satisfied our WISE criteria.

2.3. Cutouts

For each source in the overlap between WISE and ATLAS we downloaded 12'' square *ugriz* FITS subrasters (58 pixels on a side) from the University of Edinburgh Wide Field Astronomy Unit’s OmegaCam Science Archive (henceforth OSA; Hambly et al 2008; Cross et al 2012). The size of these “cutouts” was chosen to be larger than most known quasar/galaxy lens systems while minimizing the possibility of including an unrelated source in the field. These were downloaded using the unix *wget* command, following the recipe given on the OSA website. The rate limiting factor was the time to process each request (perhaps 1000 requests/hour at best) rather than the data transfer time.

2.4. Splitting blended images

For each source the available cutouts were analyzed using pieces of the DoPHOT photometry program (Schechter, Mateo and Saha 1993). DoPHOT incorporates an elliptical profile that approximates a Gaussian near the core but has broader wings.

In each of the three filters with the best seeing, as recorded in the FITS headers, we attempt to split candidates into two sources with a common quasi-Gaussian shape. From these we chose the two source fit that shows the greatest improvement over a single extended object (as measured by our goodness of fit parameter) as our “anchor” estimate of the separation between components.

For as many of the *ugriz* filters as we have cutouts, we carry out two source fits, with the separation constrained to our anchor value, but allowing the fluxes to vary along with a common set of shape parameters and an overall position. We call these separation-constrained two-source-

one-ellipse (2S1E) fits.

If the flux ratio from one of these separation-constrained fits is very different from the anchor value (3 magnitudes) at a high level of significance (10σ) we take the anchor splitting to be spurious. This frequently happens at smaller separations, at which trailed or astigmatic images can cause the object to look elongated or double in one exposure.

2.5. Weeding out galaxies

In addition to quasars, our WISE quasar-colored systems include star forming galaxies, which often come in close pairs. Moreover, with a thousand unlensed quasars for every lensed quasar, we expect accidental projections of foreground galaxies close to quasars.

Every separation-constrained two-source-one-shape fit gives us a footprint that can be compared with the seeing as recorded in the FITS header for that filter. Pairs of galaxies are expected to have larger footprints, as measured by the area of the quasi-Gaussian, than the stellar PSF. After some experimentation, we decided to eliminate as a probable galaxy pair any system for which the separation-constrained 2S1E fits were larger than the stellar PSFs by 2 square pixels in all three of the filters with the best seeing.

There is a two-source-two-ellipse (2S2E) alternative to our adopted model that allows for the further weeding out of galaxies, at the cost of adding the three additional shape parameters associated with a second elliptical Gaussian. We fit this to the filter that yielded our best split and obtain convergence for roughly 65% of our candidates. We exclude systems for which the minor axes of the two components differ by more than a factor of $\sqrt{2}$. We also exclude systems for which the minor axes differ by more than a factor of $2^{1/4}$ and for which the ratio of the areas is larger than a factor of two.

2.6. Ranking on the basis of achromaticity

The word “achromatic” is often used to describe gravitational lensing. While color may vary from one part of an extended source to another, if the source is small compared to the Einstein ring of a gravitational lens, the multiple images will all have the same color.

This is less powerful than one might hope in discriminating between lensed quasar systems and chance superpositions of objects for two reasons. First, lensed systems also include lensing galaxies, the light from which will be split disproportionately between the two images. Second, especially at brighter apparent magnitudes, the quasars are micro-lensed by the stars within the lensing galaxies and are somewhat extended compared to the micro-lensing Einstein rings. This leads to differential micro-lensing (Blackburne et al 2011).

We use the separation-constrained 2S1E flux ratios at each observed wavelength, expressed in magnitudes, δm_λ , to fit for a slope, $d\delta m_\lambda/d\log \lambda$. We adopt a rough guess of the mean slope for a lensed system $\langle \alpha \rangle = 0.217$, and of the scatter in that slope, $\sigma_\alpha = 0.325$, and score systems based on their deviation from the mean slope.² We also score systems on the absence of scatter from the observed slope and finally score systems on the consistency of the u filter flux ratio with those in the other filters. A final ranking is computed by taking the product of these three scores. Details of our scoring system (which we continue to refine as we observe more candidates) will be presented in a forthcoming paper.

2.7. Optical colors

We have argued above that catalogued optical colors may be unreliable for lensed quasar systems because catalog photometry explicitly or implicitly assumes a light distribution light over the detector pixels that is inappropriate to a lensed quasar system. Our 2S1E model should produce better (but hardly perfect) colors.

For this, our first pass through the data, we restricted ourselves to the simplest of quasar color criteria, ultraviolet excess (henceforth UVX). This works well for quasars with $z < 2.2$ (Richards et al 2001) but would exclude the roughly 25% of unlensed quasars of an SDSS-like survey at higher redshift.

Optical colors were computed adding the two fluxes from the constrained-separation 2S1E fits in each of the filters. The photometric zeropoints embedded in the OmegaCam FITS headers were used to create $u - g$ colors in a Vega-like $ugriz$ system (Shanks et al 2015). We adopted the UVX criterion $u - g < -0.5$ in which seems to exclude narrow emission line galaxies and white dwarf pairs but to include lensed quasars at $z < 2.2$.

Applying the recipe described in this section, we are left with a ranked list of candidate lensed quasar systems.

3. Spectroscopic and Direct Observations and Reductions

From June 2015 through April 2016, spectroscopic observations were carried out for roughly a dozen highly ranked systems with both the f/2 and f/4 cameras of the Inamori Magellan Areal Camera and Spectrometer, henceforth IMACS (Dressler et al 2010) on the Baade 6.5-m telescope of the Magellan telescopes. In Table 1 we give coordinates for seven of the objects observed, their rankings and colors, and descriptions of the resulting spectra.

²Fainter images are more likely to include more of the red light from the lensing galaxy.

3.1. Choice of Systems

While guided by rank, the actual choice of systems to observe also depended upon seeing, as some of the systems are quite close, and upon cloud cover. The pairs of blue stars and narrow line galaxies that predominated in our first observations led us to tighten our UVX criterion in subsequent runs.

3.2. Direct Imaging of WISE 2344-3056

The system WISE 2344-3056 was given top priority for observation in December 2015 because its appearance in the ATLAS images suggested a quadruple system. Figure 1 shows the VST ATLAS image of WISE 2344-3056 in the g filter, which gave the best splitting of the object. We have superposed the elliptical FWHM contours from the two-source-one-ellipse model.

The minor axis of the two-source-one-ellipse model is $1''.11$, slightly less than the $1''.18$ seeing reported in the image header. The major axis is $1''.41$ and elongated so that each ellipse includes two of the four images.

The system only barely survived being eliminated as a pair of galaxies, suggesting that we may need to relax the 2S2E criteria described in §2.5.

We use IMACS in a mode that requires one or more direct images to be taken to position the object in the slit. For WISE 2344-3056, the first of these, in Sloan r , confirmed the suspicion that was at least triple, so two more images were taken in Sloan i . The left panel of Figure 2 shows one of the i images, taken in $0''.55$ seeing with the $f/2$ camera.

The debiased and flatfielded frames were analyzed using the program DoPHOT (Schechter et al 1993). The standard version of the program found all four quasar images on the r frame and needed only minor nudging to find all four on the other two. The right panel of Figure 2 shows the residuals from one of those fits, using the point spread function of a nearby star as the empirical PSF. The residuals show little or no trace of a lensing galaxy.

Astrometry was carried out on one of the i frames using catalogued positions from the ATLAS survey, with rms residuals of $0''.1$. Results are given in Table 2. The four positions are indicated by the blue circles in Figure 1.

Fluxes relative to the brightest image were likewise computed using DoPHOT. These were then used to compute magnitudes assuming a combined Petrosian i magnitude of 19.15 as given in the ATLAS catalogue, which reports magnitudes in an AB system (Shanks et al 2015) rather than in the Vega-like system of the FITS headers. To the extent that the quasar has varied in the 4 years between the ATLAS and IMACS exposures, these will share a common systematic error.

3.3. Direct Imaging of WISE 0326-3122

A 30 s direct image of WISE 0326-3056 in the Sloan r filter in $0''.64$ seeing was obtained with the IMACS f/2 in setting up for spectroscopy. The debiased and flatfielded frame was analyzed with DoPHOT. Figure 3 shows the original image of the candidate system and the same image with best fitting PSFs subtracted. The residuals show little or no trace of a lensing galaxy.

3.4. Spectra

Spectra for the objects in Table 1 were obtained using either the “short” f/2 camera or “long” f/4 camera on IMACS, in both cases using a 3800-7000 Å blocking filter. Dispersers with 300 lines mm^{-1} were used on both cameras: a grism blazed at 17.5° on the short camera and a grating blazed at 4.3° on the long camera. The spectra were binned by 2 pixels in the spectral direction (except where noted) on the short camera and by 4 pixels on the long camera. On the latter, they were also binned by 2 pixels along the slit. Except where noted, the $0.9''$ slit was oriented to obtain spectra of both components of the system.

The spectra were bias-subtracted and flattened using standard procedures, and cosmic rays near the extraction paths were identified by eye and replaced with interpolated values along each row of the detector. Wavelength calibration was provided by Argon lamp lines taken a short time before each target exposure. A multi-order polynomial fit as a function of both the spatial and dispersion directions was used for the wavelength solution and gave typical fit rms values with respect to the reference line list of 0.3 \AA or better for all target chips. The dispersion ranged from 2.2 to $2.6 \text{ \AA pixel}^{-1}$ on the short camera and from 2.8 to $3.0 \text{ \AA pixel}^{-1}$ on the long camera. Sky background was subtracted using linear interpolation along each row of the detector. The spectra show gaps near 6550 \AA on the short camera and near 5300 \AA on the long camera due to the physical spacing between CCDs on the IMACS cameras.

When the seeing permitted, spectra were extracted for the individual components of each system. This was accomplished by fitting two overlapping Gaussian profiles to each spatial row of the detector. We first performed a preliminary fit of overlapping Gaussian profiles for the brighter and fainter components for each row. The separation and brightness of each component were free to vary, as well as the common FWHM used for both profiles. Using these results, a polynomial fit to the brighter component’s center as a function of CCD row provided a trace path for the final extraction. During the final extraction, the overall position was dictated by the trace path and the relative separation was held fixed at the average value from the preliminary fit. In this way, only the brightness of the A and B profiles and the common FWHM were free to vary for each row during the final extraction.

Figures 4-6 show the extracted spectra for the objects in Table 1. The displayed spectra were top-hat smoothed using a 3 pixel window in the dispersion direction for cosmetics; Gaussian

profile fitting was performed on the unsmoothed spectra. We were able to extract individual spectra for WISE 0145-1327, WISE 0326-3122, WISE 1051-1142, WISE 1427-0715, WISE 2215-3056, and WISE 2329-1258. For these systems an inset at lower right of each plot shows the Gaussian decomposition of the two components for a single CCD row of the detector. The small separation of WISE 2344-3056 precluded decomposing the combined spectra. Instead, we used a simple constant-width extraction window of $2.2''$ centered on the trace path.

4. Interpretation of Spectra

4.1. Binary quasar, lensed quasar, or nearly identical quasar pair?

The words “binary quasar” are used to describe two distinct quasars at the same redshift, as opposed to two images of a single lensed quasar (Hennawi et al 2006). But when one observes a pair of quasars, conclusive discrimination between these two alternatives is not always straightforward (Wisotzki et al 1993; Muñoz et al 1997; Mortlock et al 1997).

The history of HE1104-1805 is instructive in this regard. Wisotzki and collaborators (1993) found that the two components differed in the slopes of their continua and in the equivalent widths of their emission lines, but that the shapes of their emission lines were identical. They argued that the spectral differences might be due to micro-lensing by stars in the lensing galaxy. But they detected no lensing galaxy at $R \lesssim 24$. Wisotzki et al (1995) subsequently observed correlated changes in the continuum flux of the two systems, which they took as confirmation of the lensing hypothesis. Courbin et al (1998) conclusively detected the lensing galaxy, much closer to the brighter image than might naively have been expected. Crude interpolation between subsequent HST observations (Remy et al 1998) would give $R \sim 22$ for the lensing galaxy. Lidman et al (2000) measured a lens redshift of $z = 0.729$.

The circumstances of three of our systems are similar to those of HE1104-1805 in 1993. The spectra differ, but no more than they might under the micro-lensing hypothesis. Still, no lensing galaxy is observed. We think it premature to call such systems binary quasars, and instead refer to them as “nearly identical quasar pairs.” If lensing galaxies or correlated variations are ultimately observed, they will be classified as lens systems.

But if only upper limits can be measured for a lensing galaxy, careful modeling is needed to establish that those upper limits are inconsistent with plausible lensing scenarios. Alternatively, higher signal-to-noise spectra or spectra of narrow emission lines might show significant differences in the line profiles or redshifts, ruling out the lensed system hypothesis.

In the sequel to the SQLS, the SDSS-III BOSS Quasar Lens Survey, More et al (2016) are similarly circumspect in not drawing strong conclusions about nearly identical quasar pairs for which no lensing galaxy is observed.

4.2. WISE 0145-1327: a projected pair

WISE 0145-1327 is a chance projection of two quasars. The brighter of the pair is at a redshift of $z = 1.0903 \pm 0.0004$ from a Gaussian fit to the MgII emission line. The fainter object is at a higher redshift of $z = 1.9748 \pm 0.0005$ based on its CIV broad emission line. The spectra are shown in Figure 4.

4.3. WISE 0326-3122: a nearly identical pair at $z = 1.34$

The two quasar images of WISE 0326-3122 have nearly identical redshifts and spectral flux ratios. Both show a CIII] broad emission line at around 4460 Å. Gaussian fits to the CIII] profiles yield identical source redshifts of $z = 1.3366 \pm 0.0014$ for the brighter object and $z = 1.3375 \pm 0.0021$ for the fainter object. This redshift places the MgII broad emission line inside the IMACS chip gap with only a hint of the feature’s wing visible for the brighter component. There is also a MgII $\lambda\lambda 2796, 2803$ absorption doublet at $z = 0.5080 \pm 0.0001$ present in the brighter component’s spectrum. The flux ratio between components is also remarkably constant at about 3.2:1 (0.5 dex in Figure 4) over the entire IMACS spectral range. This makes it all the more surprising that no lensing galaxy is observed in the star subtracted image (Figure 3).

4.4. WISE 1051-1142: a nearly identical pair at $z = 0.88$

The two quasar images of WISE 1051-1142 have nearly identical redshifts. The MgII broad emission line is present for both components just blueward of the IMACS chip gap. Gaussian fits to the emission profiles yield source redshifts of $z = 0.8828 \pm 0.0003$ and $z = 0.8789 \pm 0.0011$ for the brighter and fainter components, respectively, which overlap at the $3-4\sigma$ level. There are no obvious signs of intervening absorption. The flux ratio between components varies from 5:1 (0.7 dex in Figure 5) at the blue end to 8:1 (0.9 dex) at the red end, not inconsistent with wavelength-dependent continuum microlensing seen in other lensed quasars.

4.5. WISE 1427-0715: a projected pair

WISE 1427-0715 is a chance projection of two quasars. The brighter component shows the MgII broad emission line at about 6230 Å yielding a source redshift of $z = 1.2257 \pm 0.0004$. The fainter component has its MgII broad emission line at about 4820 Å and yields a source redshift of $z = 0.7219 \pm 0.0004$. A MgII $\lambda\lambda 2796, 2803$ absorption doublet is also seen in the brighter component’s spectrum at a fitted redshift of $z = 0.7204 \pm 0.0001$ and thus associated with the host galaxy of the fainter quasar. The spectra are shown in Figure 5.

4.6. WISE 2215-3056: a binary quasar at $z = 1.34$

WISE 2215-3056 is a binary quasar. Its components have similar redshifts but have notable spectral differences. The brighter component is at $z = 1.3476 \pm 0.0003$ based on its MgII broad emission line profile and shows strong BAL features blueward of its CIII] and MgII emission lines. The fainter component has a source redshift of $z = 1.3503 \pm 0.0005$ based on its MgII profile, about a 5σ difference from the brighter component, but shows none of the corresponding BAL features. There is also a prominent FeIII/UV 48 broad emission line of comparable intensity to CIII] in the brighter component that is lacking in the fainter companion. Despite the similar redshifts, the spectral differences argue for two separate quasars. The spectra are shown in Figure 5.

4.7. WISE 2329-1258: a nearly identical pair at $z = 1.31$

The two quasar images of WISE 2329-1258 have nearly identical redshifts with a rich set of absorption features present in both spectra. The MgII broad emission line is at $z = 1.3102 \pm 0.0008$ for the brighter component and $z = 1.3146 \pm 0.0018$ for the fainter component, overlapping at the $2\text{-}3\sigma$ level. A similar agreement is seen for the CIII] broad emission line. The narrow-line absorption features present in the spectra of both components can be modeled with two absorbers at $z = 1.1526 \pm 0.0001$ and $z = 0.7644 \pm 0.0001$. Both are anchored by an appropriately redshifted MgII $\lambda\lambda 2796,2803$ doublet and accompanying FeII $\lambda\lambda 2382, 2600$ absorption lines. We also identify FeII $\lambda\lambda 2344, 2374$ and 2586 for the $z = 1.1526$ absorber. The flux ratio between the components is also remarkably constant at about 2.5:1 (0.4 dex in Figure 6) over the entire IMACS spectral range.

4.8. WISE 2344-3056: a quad at $z = 1.30$

The small size of WISE 2344-3056 made it impractical to extract individual spectra for the lensed quasars and we only present the combined spectrum in Figure 6. The quasar redshift is $z = 1.2981 \pm 0.0002$ based on a Gaussian fit to the MgII broad emission line. The CIII] broad emission line is also present at a much lower signal to noise. There is at least one intervening absorption system at $z = 0.9467 \pm 0.0001$ anchored by the MgII $\lambda\lambda 2796,2803$ absorption doublet, several FeII lines ($\lambda\lambda 2344,2374,2382,2399,2586,2600$), FeIII $\lambda 2419$, and MgI $\lambda 2852$.

5. A lens model for WISE 2344-3056

We used Keeton’s `lensmodel` program (2001) to fit a singular isothermal sphere with external shear to the astrometry for WISE 2344-3056 given in Table 2. As we do not detect the lensing galaxy, the center of the lens is left free and found to be $0''.436$ west and $0''.151$ north of image A.

The model puts the source $0''.441$ west and $0''.153$ north of image A. The external shear is 0.063 and is directed along P.A. 18.5° . The signed magnifications for images A, B, C and D are, respectively, -6.8, 8.4, 8.6, -8.1.

6. Discussion

We have argued that it is premature to classify any three of our nearly identical quasar pairs as binary quasars rather than single lensed quasars, despite the fact that no lensing galaxy has as yet been identified. In Figure 7 we show the three systems, with the component spectra shifted to overlap. For WISE 0326-3122 and WISE 2329-1258 the agreement is nearly perfect, while for WISE 1051-1142 the differences are consistent with what one would expect for a micro-lensed system.

With sufficiently deep direct images in sufficiently good seeing one can set upper limits on the lensing galaxy that rule out the lensing hypothesis, but only with extensive modeling of lensing scenarios. If higher signal-to-noise spectra, or spectra at other wavelengths were to show significant differences in the line profiles, they would again rule out the lensing hypothesis. Confirmation of the lensing hypothesis might come either from identification of the lensing galaxy or from correlated variations in the fluxes, as might be obtained from synoptic observations with the LSST.

REFERENCES

- Agnello, A., Treu, T., Ostrovski, F., et al. 2015, MNRAS, 454, 1260
- Agol, E., & Krolik, J. 1999, ApJ, 524, 49
- Blackburne, J. A., Pooley, D., Rappaport, S., & Schechter, P. L. 2011, ApJ, 729, 34
- Courbin, F., Lidman, C., & Magain, P. 1998, A&A, 330, 57
- Cross, N. J. G., Collins, R. S., Mann, R. G., et al. 2012, A&A, 548, A119
- Dressler, A., Bigelow, B., Hare, T., et al. 2011, PASP, 123, 288
- Hambly, N. C., Collins, R. S., Cross, N. J. G., et al. 2008, MNRAS, 384, 637
- Hennawi, J. F., Strauss, M. A., Oguri, M., et al. 2006, AJ, 131, 1
- Holder, G. P., & Schechter, P. L. 2003, ApJ, 589, 688
- Inada, N., Oguri, M., Shin, M.-S., et al. 2012, AJ, 143, 119
- Jiménez-Vicente, J., Mediavilla, E., Kochanek, C. S., & Muñoz, J. A. 2015, ApJ, 799, 149
- Kayser, R., Refsdal, S., & Stabell, R. 1986, A&A, 166, 36
- Keeton, C. R. 2001, arXiv:astro-ph/0102340
- Kochanek, C. S., Falco, E. E., & Muñoz, J. A. 1999, ApJ, 510, 590
- Lidman, C., Courbin, F., Kneib, J.-P., et al. 2000, A&A, 364, L62
- Marshall, P. J., Treu, T., Melbourne, J., et al. 2007, ApJ, 671, 1196
- Morgan, N. D., Caldwell, J. A. R., Schechter, P. L., Dressler, A., Egami, E., & Rix, H. 2004, AJ, 127, 2617
- Mortlock, D. J., Webster, R. L., & Francis, P. J. 1999, MNRAS, 309, 836
- Pooley, D., Blackburne, J. A., Rappaport, S., & Schechter, P. L. 2007, ApJ, 661, 19
- Pooley, D., Rappaport, S., Blackburne, J. A., Schechter, P. L., & Wambsganss, J. 2012, ApJ, 744, 111
- Rauch, K. P., & Blandford, R. D. 1991, ApJ, 381, L39
- Remy, M., Claeskens, J.-F., Surdej, J., et al. 1998, New A, 3, 379
- Richards, G. T., Fan, X., Schneider, D. P., et al. 2001, AJ, 121, 2308

- Schechter, P. L., Pooley, D., Blackburne, J. A., & Wambsganss, J. 2014, *ApJ*, 793, 96
- Schechter, P. L., Mateo, M., & Saha, A. 1993, *PASP*, 105, 1342
- Schechter, P. L., & Wambsganss, J. 2002, *ApJ*, 580, 685
- Schechter, P. L., & Wambsganss, J. 2004, in *IAU Symposium*, Vol. 220, *Dark Matter in Galaxies*, ed. S. Ryder, D. Pisano, M. Walker, & K. Freeman, 103–+
- Schneider, P. 2006, *Saas-Fee Advanced Course 33: Gravitational Lensing: Strong, Weak and Micro*, 91
- Shanks, T., Metcalfe, N., Chehade, B., et al. 2015, *MNRAS*, 451, 4238
- Sérsic, J. L. 1963, *Boletin de la Asociacion Argentina de Astronomia La Plata Argentina*, 6, 41
- Sluse, D., Schmidt, R., Courbin, F., et al. 2011, *A&A*, 528, A100
- Stern, D., Assef, R. J., Benford, D. J., et al. 2012, *ApJ*, 753, 30
- Treu, T., & Marshall, P. J. 2016, [arXiv:1605.05333](https://arxiv.org/abs/1605.05333)
- Wambsganss, J. 2006, *Gravitational Microlensing*, ed. Schneider, P., Kochanek, C. S., & Wambsganss, J., 453–+
- Wright, E. L., Eisenhardt, P. R. M., Mainzer, A. K., et al. 2010, *AJ*, 140, 1868-1881

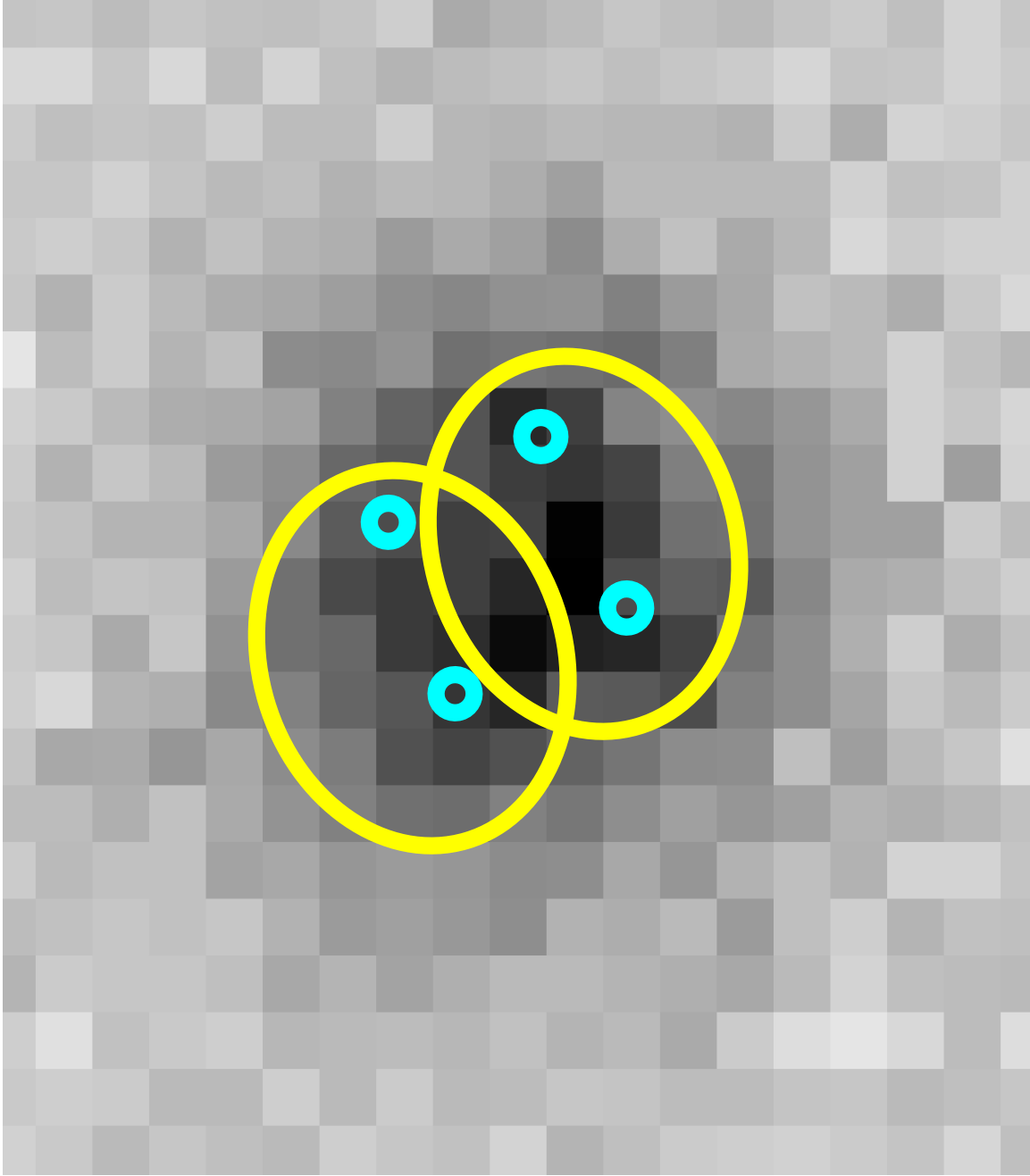


Fig. 1.— The VST-ATLAS *g* stack for WISE 2344-3056. The yellow ellipses are the result of our two-source-one-shape splitting of this source. The blue circles are at the positions of the four images (D, C, B and A from left to right) identified with IMACS. The scale is $0''.213$ per pixel. North is up and East is to the right.

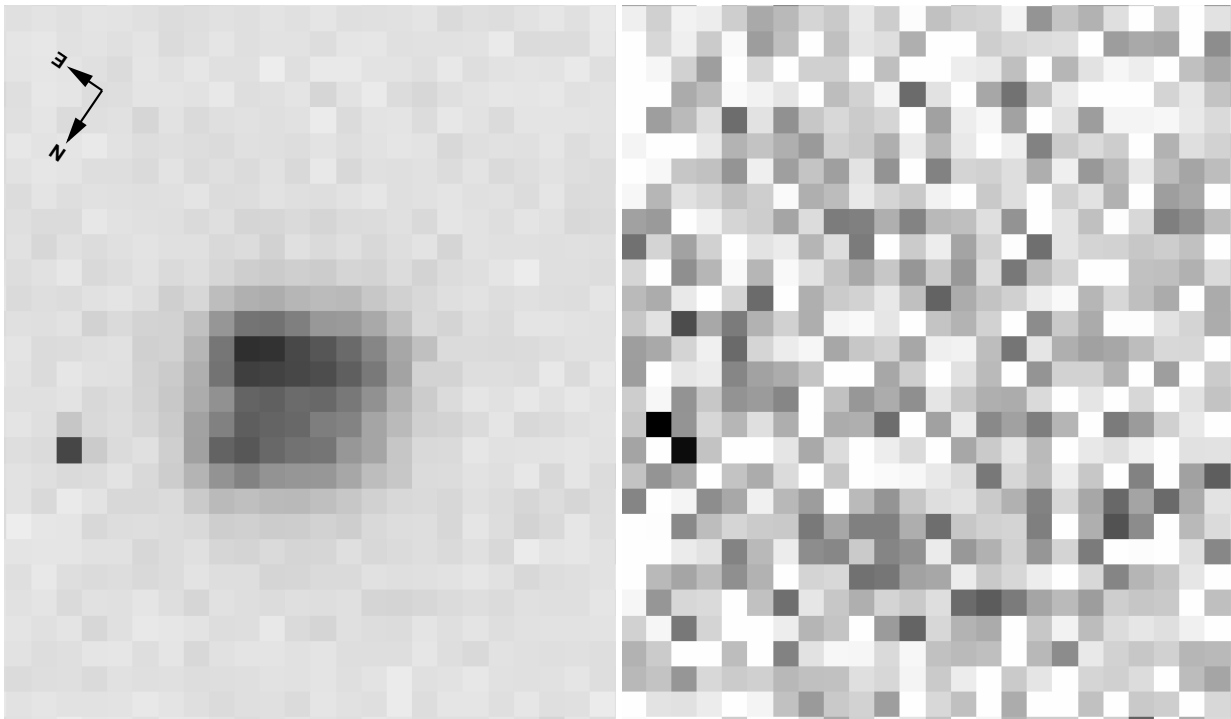


Fig. 2.— Left: A 60s *i* exposure of WISE 2344-3056 taken with IMACS in $0''.55$ seeing. Right: the same exposure, with four point sources subtracted, at 10 times higher contrast. The scale is $0''.200$ per pixel

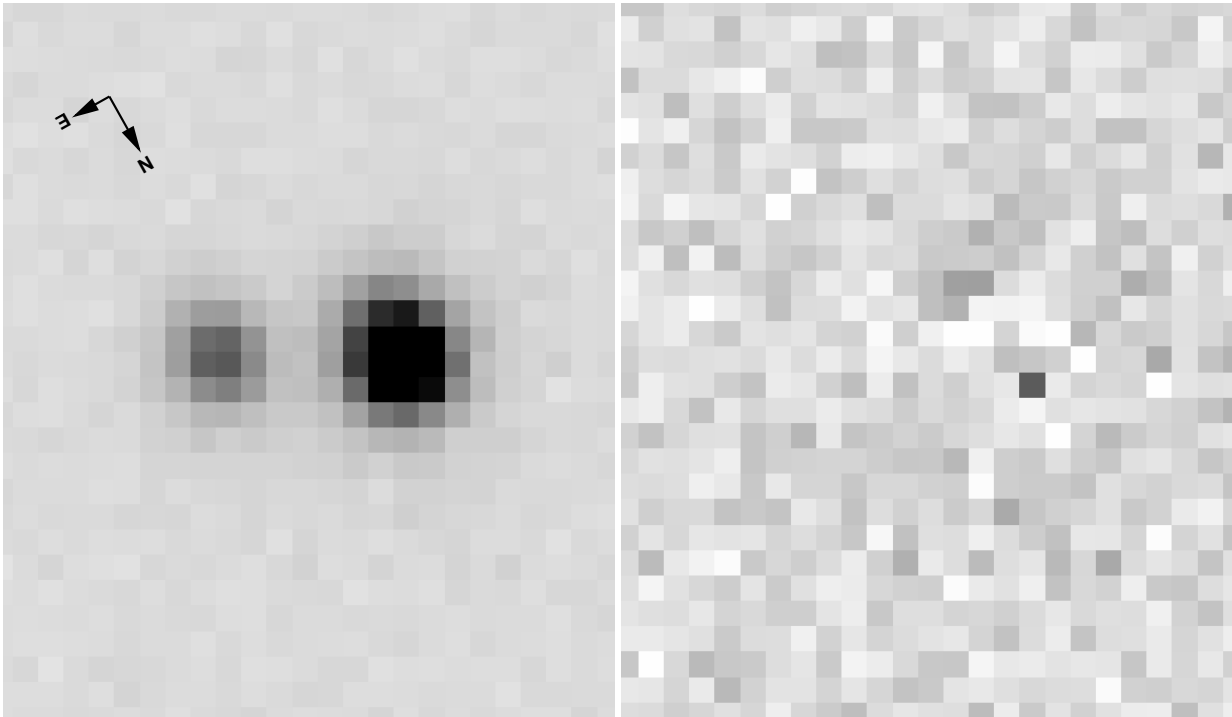


Fig. 3.— Left: A 30s Sloan *r* exposure of WISE 0326-3122 in $0''.64$ seeing. Right: the same exposure, with two point sources subtracted, at 5 times higher contrast. The scale is $0''.200$ per pixel.

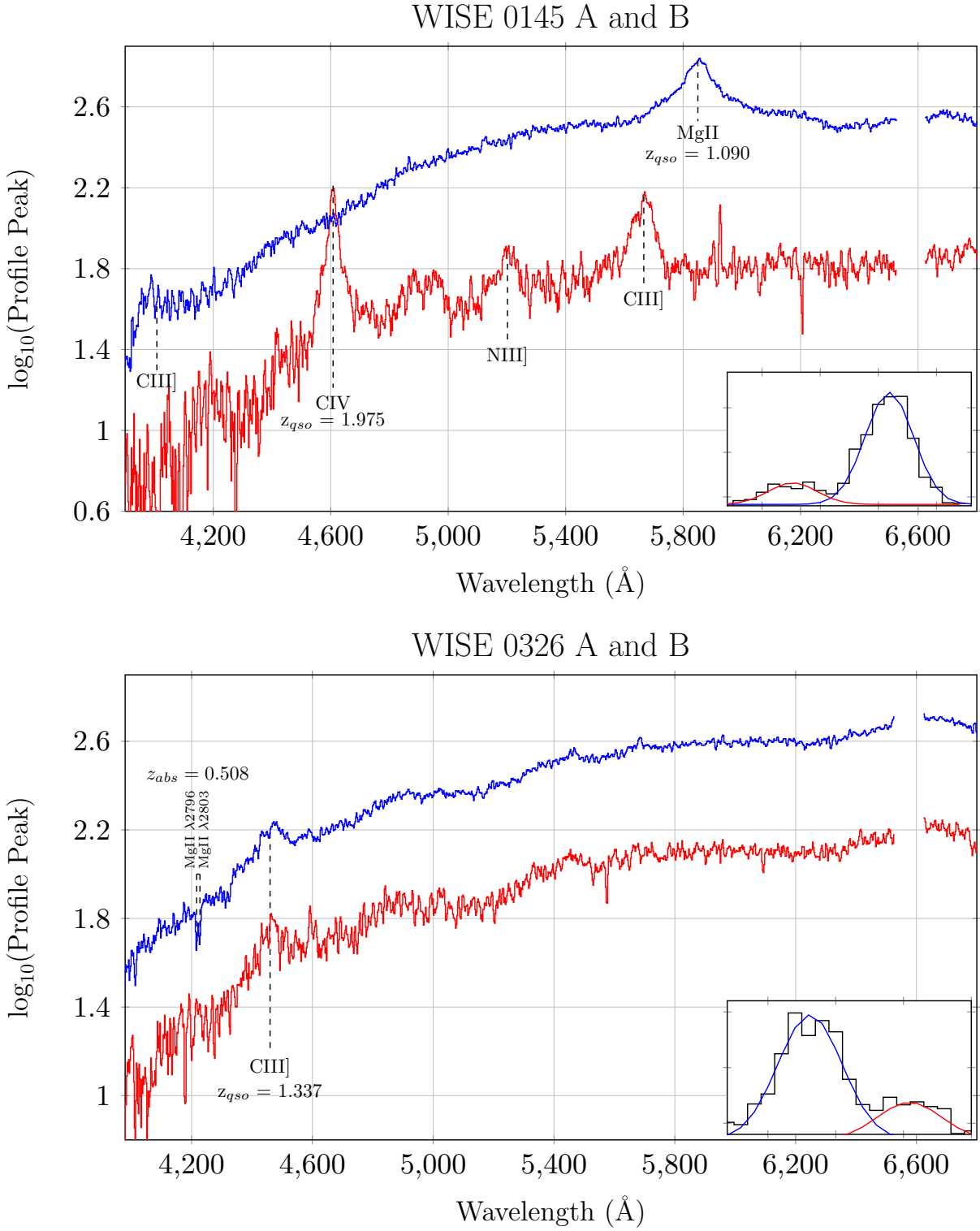


Fig. 4.— Spectra of WISE 0145-1327 and WISE 0326-3122 taken with IMACS

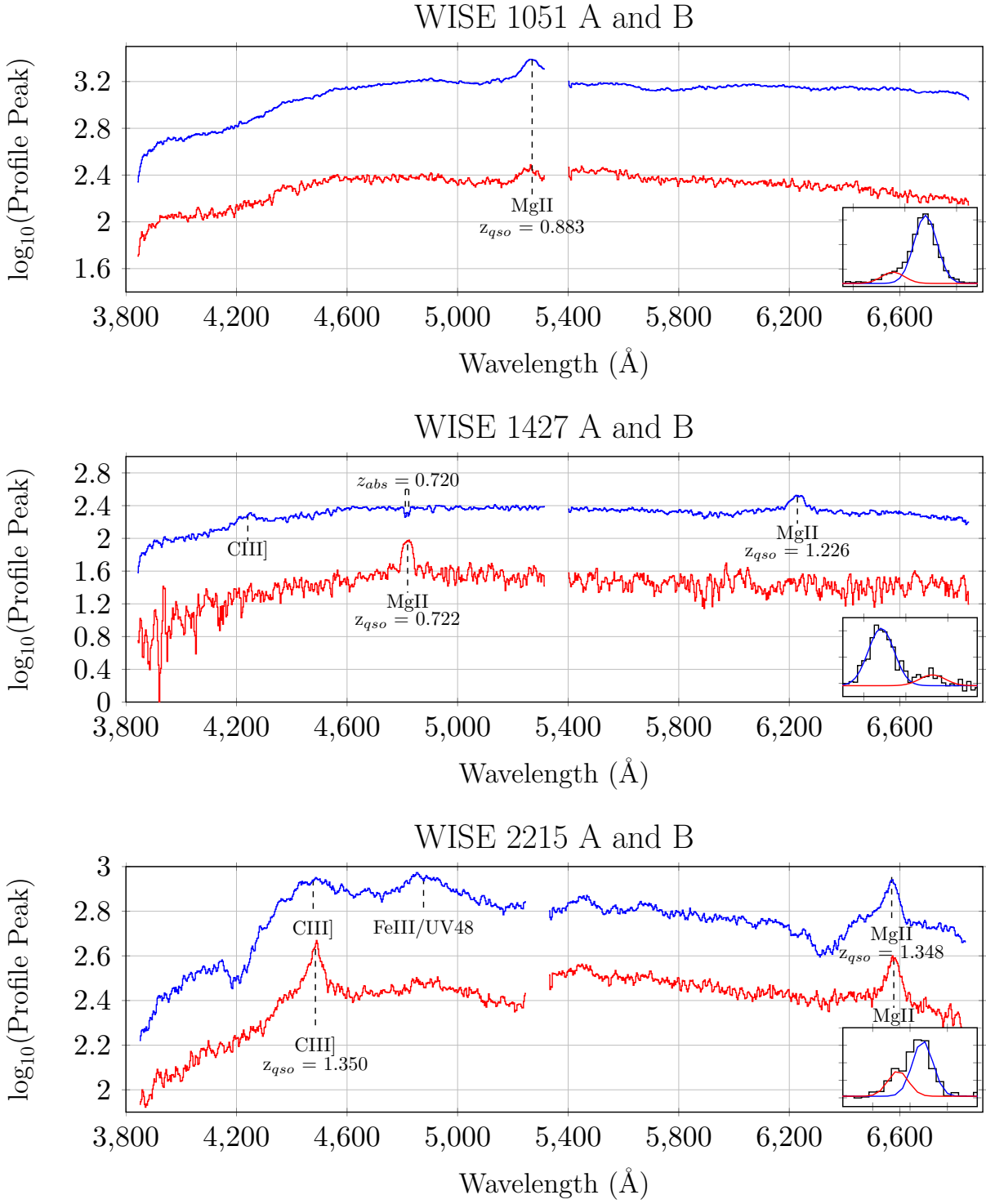


Fig. 5.— Spectra of WISE 1051-1142, WISE 1427-0715 and WISE 2215-3056 taken with IMACS

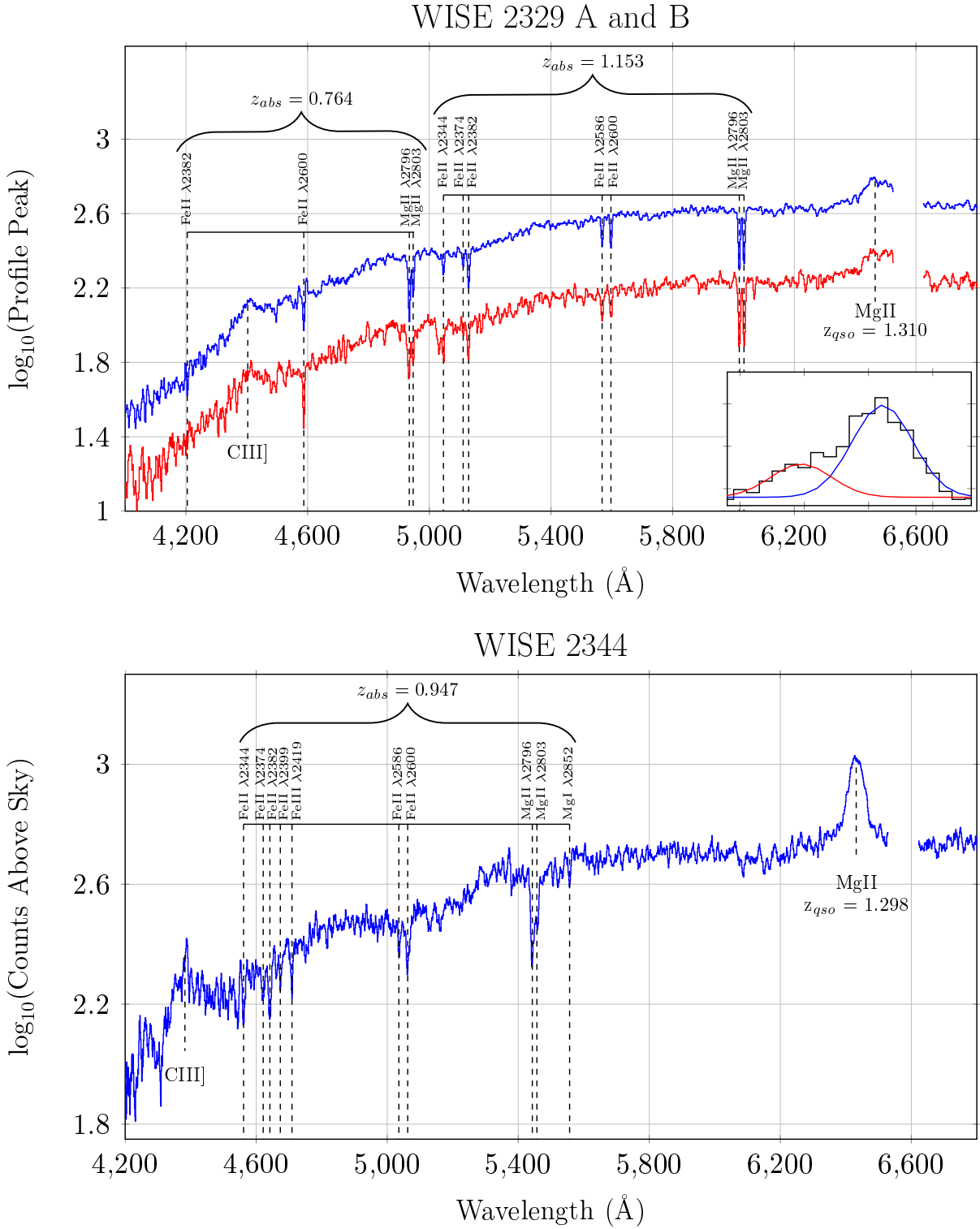


Fig. 6.— Spectra of WISE 2329-1258 and WISE 2344-3056 taken with IMACS

Superposed Spectra for Nearly Identical Systems

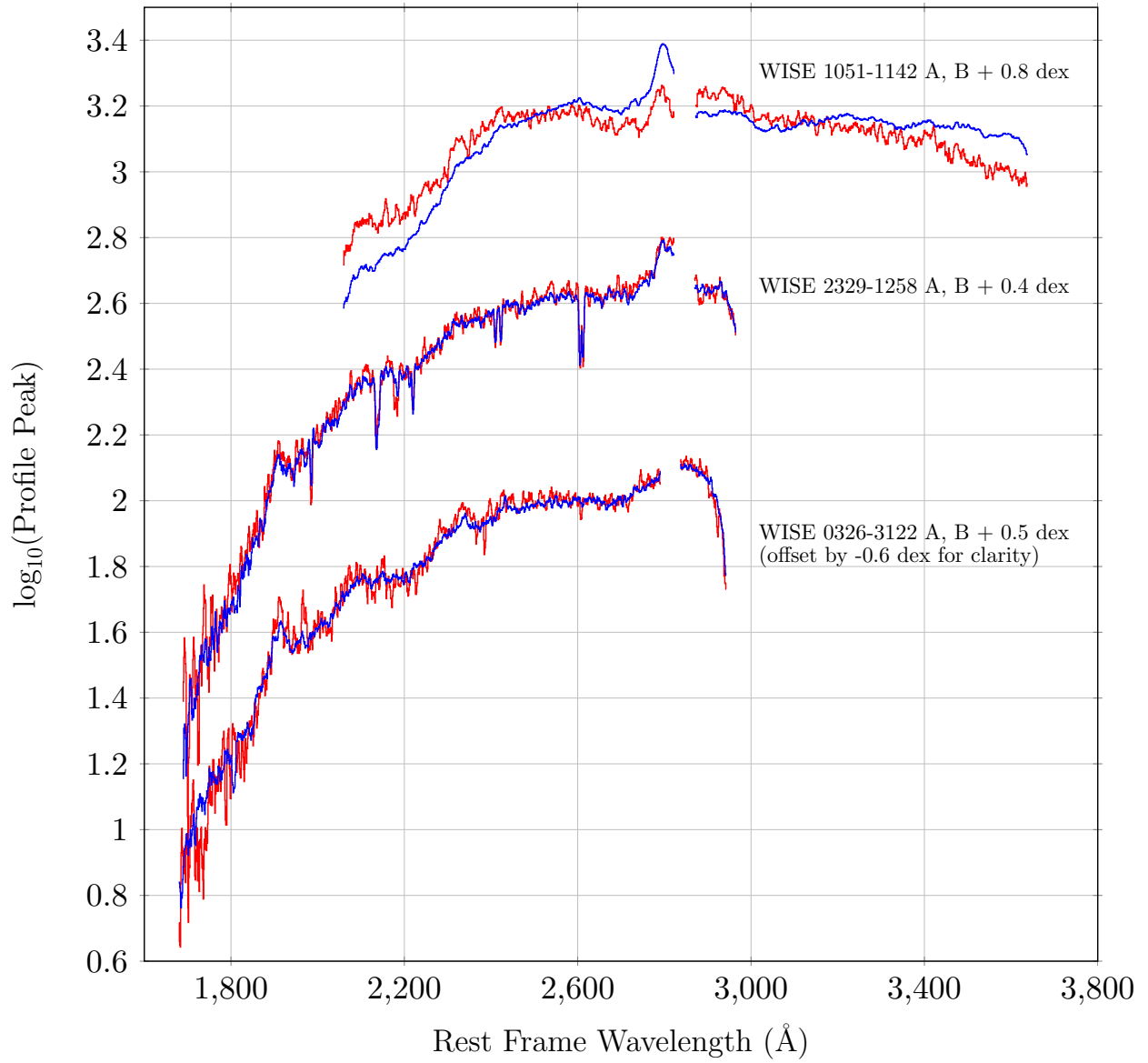


Fig. 7.— Rest frame spectra of WISE 0326-3122, WISE 1051-1142 and WISE 2329-1258, with the *A* and *B* components superposed.

Table 1. Spectroscopic Observations of Lensed Quasar Candidates

R.A.	$\Delta\theta$	i_A^*	score	camera	description	
Dec.	P.A.	i_B^*	$(u - g)^\dagger$	exp.	redshift(A/B)	
01 45 25.3	1''68	19.25	0.39	f/2	projected	
–13 27 25	5°	20.59	-1.01	1200s	1.09/1.97	
03 26 06.8	1''43	19.49	0.60	f/2	nearly identical	
–31 22 54	–60°	20.56	-1.17	1200s	1.34	
10 51 41.9	1''47	17.25	0.50	f/4	nearly identical	
–11 42 39	–5°	19.39	-0.89	900s	0.88	
14 27 04.8	2''80	18.92	0.49	f/4	projected	
–07 15 56	9°	20.32	-0.73	900s	1.23/0.72	
22 15 25.6	0''71	18.31	0.29	f/4	binary	
–30 56 35	–41°	19.07	-0.61	900s	1.34	
23 29 57.9	1''27	17.63	0.96	f/2	nearly identical	
–12 58 59	46°	18.60	-0.82	600s	1.314	
23 44 17.0		20.31 [‡]	0.44	f/2	quadruple	
–30 56 26		20.63 [‡]	-0.63	900s	1.298	

*magnitudes for A and B components derived from catalogued ATLAS Petrosian AB magnitudes and 2S1E flux ratios,.

[†] $u - g$ colors are in the Vega-like system of the ATLAS FITS headers

[‡] $i_C = 20.71$ and $i_D = 21.12$

Table 2. Astrometry and Photometry for WISE 2344-3056

image	$\Delta\alpha$	$\Delta\delta$	i^*
A	0''000	0''000	20.31
B	-0''304	0''665	20.63
C	-0''641	-0''337	20.71
D	-0''886	0''293	21.12

*Positions relative to
 $\alpha_A = 23^h 44^m 16''.995$ and
 $\delta_A = -30^\circ 56' 26''.22$